

Resolution of a bent-crystal spectrometer for X-ray free electron laser pulses: diamond vs. silicon

Vladimir M. Kaganer,^a Ilia Petrov^b and Liubov Samoylova^b^aPaul-Drude-Institut für Festkörperelektronik, Leibniz-Institut im Forschungsverbund Berlin e. V., Hausvogteiplatz 5–7, 10117 Berlin, Germany, and ^bEuropean XFEL GmbH, Holzkoppel 4, 22869 Schenefeld, Germany

The resolution function of a spectrometer based on a strongly bent single crystal (bending radius of 10 cm or less) is evaluated. It is shown that the resolution is controlled by two parameters, (i) the ratio of the lattice spacing of the chosen reflection to the crystal thickness and (ii) a single parameter comprising crystal thickness, its bending radius, and anisotropic elastic constants of the chosen crystal. Diamond, due to its unique elastic properties, can provide notably higher resolution than silicon. The results allow to optimize the parameters of bent crystal spectrometers for the hard X-ray free electron laser sources.

Keywords: x-ray free-electron lasers; x-ray spectroscopy; bent crystals; diamond crystal optics; femtosecond x-ray diffraction.

© 2020 International Union of Crystallography
Printed in Singapore – all rights reserved

1. Introduction

The self-amplified spontaneous emission (SASE) radiation pulse of an X-ray free-electron laser (XFEL) originates from random current fluctuations in the electron bunch and have an individual time structure (Saldin *et al.*, 2000). Detectors that could resolve the time structure of a femtosecond pulse are neither available nor expected in the near future. The measurement of the energy spectrum of an individual pulse provides information on its time structure.

A pulse consists of 0.1 fs spikes, which results in an energy range to be covered by a spectrometer of about 40 eV. A pulse duration of 50 fs gives rise to a required energy resolution of 0.08 eV. These requirements are matched by using Bragg diffraction on a thin single crystal bent to a radius of 10 cm or less. Spectrometers based on bent silicon (Zhu *et al.*, 2012; Makita *et al.*, 2015) and diamond (Boesenberg *et al.*, 2017; Samoylova *et al.*, 2019) crystals have been reported so far.

Recently, we have given a detailed theoretical description of the x-ray diffraction on strongly bent crystals (Kaganer *et al.*, 2020). It has been proven that the kinematical diffraction approximation can be applied in a broad range of the crystal curvatures and the X-ray energies. The diffracted intensity has been calculated. In modeling diffraction of the XFEL pulses, it has been presumed that the scattering amplitudes for different frequencies add up coherently.

In the present work, we thoroughly analyze the diffracted intensity integrated over the pulse duration. We find that the coherent sum of the amplitudes describes an instant diffraction signal. In the time-integrated signal, the intensities, rather than the amplitudes, of different frequencies add up. Afanasev & Kohn (1977) arrived at a similar conclusion when analyzing diffraction from a continuous incoherent X-ray source and averaging over random time instants of the emission of individual atoms.

We show that the spectral resolution of a bent-crystal spec-

trimeter is controlled by two parameters. One parameter is simply the ratio of the lattice spacing of the actual reflection to the crystal thickness. The other parameter depends on the crystal thickness, its bending radius, and the anisotropic elastic constants of the crystal. The elastic properties of diamond make this material particularly suitable for a bent-crystal spectrometer.

2. Time-integrated diffraction intensity

The transverse coherence length of an XFEL pulse is about 1 mm, large compared to the size of the diffraction region on a strongly bent crystal. Hence, we assume full transverse coherence of the incident XFEL pulse and take into consideration only its time structure. The electric field of the pulse can be represented by its spectrum

$$E^{\text{in}}(\mathbf{r}, t) = \int_{-\infty}^{\infty} \tilde{E}^{\text{in}}(\omega) e^{i\mathbf{k}\mathbf{s}_0 \cdot \mathbf{r} - i\omega t} d\omega. \quad (1)$$

Here ω is the frequency of a plane-wave component, $k = \omega/c$ is its wavevector, c is the speed of light, and \mathbf{s}_0 is the unit vector in the direction of the wave propagation.

The wave packet (1) is incident on a bent-crystal spectrometer. It has been proven by Kaganer *et al.* (2020) and discussed below, that the Bragg diffraction in a strongly bent crystal can be described, in a wide range of the X-ray energies and bending radii, in the kinematical (first Born) approximation. In this approximation, the amplitude of the scattered wave is [see, e.g., Born & Wolf (2019), Sec. 13.1.2]

$$E^{\text{out}}(r\mathbf{s}, t) = \frac{r_e}{r} \int_{-\infty}^{\infty} \tilde{E}^{\text{in}}(\omega) e^{i\mathbf{k}r - i\omega t} f_1(\mathbf{s}, \mathbf{s}_0; k) d\omega. \quad (2)$$

Here r_e is the classical radius of electron and \mathbf{s} is the unit vector in the direction to the detector. The distance r from the bent-crystal spectrometer to a detector is assumed large enough, so that the conditions of the Fraunhofer diffraction are satisfied.

The scattering amplitude in the first Born approximation is

$$f_1(\mathbf{s}, \mathbf{s}_0; k) = \int_V \varrho(\mathbf{r}') e^{-ik(\mathbf{s}-\mathbf{s}_0)\cdot\mathbf{r}'} d\mathbf{r}', \quad (3)$$

the integration is performed over the crystal volume, and $\varrho(\mathbf{r}')$ is the electron density of the crystal. For X-rays, it is not averaged over the physically infinitely small volumes but possesses the crystal lattice periodicity [see, e.g., Landau & Lifshitz (1984), §124]. We have restored in Eq. (2) the time exponent $\exp(-i\omega t)$, which is usually omitted when considering diffraction of a monochromatic wave, and explicitly noted in Eq. (3) the dependence of the scattering amplitude f_1 on the length of the wavevector k .

The intensity of the scattered wave at the time instant t is

$$\begin{aligned} I(rs, t) &= |E^{\text{out}}(rs, t)|^2 \\ &= \frac{r_e^2}{r^2} \iint_{-\infty}^{\infty} d\omega_1 d\omega_2 e^{i(\omega_2 - \omega_1)t} e^{i(k_1 r - k_2 r)} \\ &\quad \times \tilde{E}^{\text{in}}(\omega_1) \tilde{E}^{\text{in}*}(\omega_2) f_1(\mathbf{s}, \mathbf{s}_0; k_1) f_1^*(\mathbf{s}, \mathbf{s}_0; k_2), \end{aligned} \quad (4)$$

where the asterisk denotes the complex conjugate and $k_n = \omega_n/c$ are the wavevectors ($n = 1, 2$).

Available X-ray detectors cannot resolve the time structure within the pulse duration (otherwise, the time structure of the pulse would be measured directly without a spectrometer). Hence, the measured intensity is a result of integration over the pulse duration:

$$\mathcal{I}(rs) = \int_{-\infty}^{\infty} I(rs, t) dt. \quad (5)$$

Integration of the time-dependent term in Eq. (4) gives rise to a delta-function $\delta(\omega_1 - \omega_2)$, so that the intensity integrated over the time is

$$\mathcal{I}(rs) = \frac{2\pi r_e^2}{r^2} \int_{-\infty}^{\infty} |f_1(\mathbf{s}, \mathbf{s}_0; k)|^2 |\tilde{E}^{\text{in}}(\omega)|^2 d\omega. \quad (6)$$

This equation replaces Eq. (17) by Kaganer *et al.* (2020), where a coherent superposition of the waves with different wave vectors has been presumed.

Let us calculate now the wave vector transfer $k\mathbf{s} - (k\mathbf{s}_0 + \mathbf{Q})$ for Bragg diffraction at the reciprocal lattice vector \mathbf{Q} . Let the scattering plane be the xz plane with the x axis tangent to the surface of the bent crystal at $x = 0$ and the z axis along the inner surface normal. All plane wave components of the X-ray pulse are incident onto the crystal at the same angle $\bar{\theta}_B$ with respect to x axis.

Then, the wavevector of the incident wave is

$$\mathbf{K}^{\text{in}} = k\mathbf{s}_0 = k(\cos \bar{\theta}_B, \sin \bar{\theta}_B). \quad (7)$$

The angle $\bar{\theta}_B$ is the Bragg angle for a reference frequency $\bar{\omega}$ arbitrarily chosen in the pulse spectrum. The Bragg law reads $d \sin \bar{\theta}_B = \pi/\bar{k}$, where $\bar{k} = \bar{\omega}/c$ is the wavevector for the reference frequency and d is the lattice spacing of the chosen reflection.

The diffracted intensity is measured as a function of the angle θ between the x axis and the vector \mathbf{s} . Hence, the wavevector of the diffracted wave is

$$\mathbf{K}^{\text{out}} = k\mathbf{s} = k(\cos \theta, -\sin \theta). \quad (8)$$

With the reciprocal lattice vector $\mathbf{Q} = (0, -2\bar{k} \sin \bar{\theta}_B)$, the Bragg law $\mathbf{K}^{\text{out}} = \mathbf{K}^{\text{in}} + \mathbf{Q}$ is satisfied at the reference frequency $\bar{\omega}$. For all other frequencies presented in the incident pulse, the deviations from the Bragg law $\mathbf{q} = \mathbf{K}^{\text{out}} - (\mathbf{K}^{\text{in}} + \mathbf{Q})$ can be calculated using Eqs. (7) and (8).

It is convenient to consider the scattering angle $\bar{\theta}_B + \theta$ as twice the Bragg angle of a wave with the frequency ω' defined by this condition. The Bragg law reads $d \sin [(\bar{\theta}_B + \theta)/2] = \pi/k'$, where k' is the respective wavevector. A straightforward calculation [see also Appendix B by Kaganer *et al.* (2020)] gives $q_z = 2(k' - k) \sin \bar{\theta}_B$. We will see in the next section that q_x is not involved in further calculations.

Therefore, the squared scattering amplitude $|f_1(\mathbf{s}, \mathbf{s}_0; k)|^2$ in Eq. (6) is a function of the difference $\omega' - \omega$. We denote this function (with the factor $2\pi r_e^2/r^2$ included in it) as $R(\omega' - \omega)$ and rewrite Eq. (6) as a convolution integral

$$\mathcal{J}(\omega') = \int_{-\infty}^{\infty} R(\omega' - \omega) |\tilde{E}^{\text{in}}(\omega)|^2 d\omega. \quad (9)$$

Here $\mathcal{J}(\omega')$ is the intensity (6) after the change of variables from θ to ω' . One can see that if the resolution is ideal [i.e., $R(\omega' - \omega)$ is a delta function], the spectrum of the diffracted waves in the ω' scale coincides with the spectrum of the incident wave. That justifies the choice of the variables. Calculation of the function $R(\omega' - \omega)$ for Bragg diffraction from a bent crystal is performed in the next section.

3. Resolution of a bent-crystal spectrometer

The applicability limits of the kinematical approximation to Bragg diffraction from strongly bent crystals have been established by Kaganer *et al.* (2020). It has been shown that a bent crystal diffracts kinematically if the bending radius is so small that the X-ray beam remains at diffraction condition, i.e., within the Darwin width of the respective reflection $\Delta\theta_B$, over a distance in the direction of its propagation small compared to the extinction length Λ . This condition is satisfied as long as the bending radius is small compared to a critical radius $R_c = \Lambda/\Delta\theta_B$. For hard X-rays with energies larger than 8 keV, the kinematical approximation is applicable for the bending radii below 10 cm and the usually employed reflections of silicon and diamond.

The bending gives rise to a displacement field $\mathbf{u}(\mathbf{r})$ in the crystal. For the symmetric Bragg reflections considered in the present work, only u_z component of the displacement field is of interest. For a crystal cylindrically bent to a radius R , it is $u_z = (x^2 + \alpha z^2)/2R$. To achieve a cylindrical bending of a rectangular plate, the bending momenta have to be applied to the perpendicular edges of the plate. The same bending state can be approached by applying momentum to the apex of a triangle-shaped plate (Terentyev *et al.*, 2016). The parameter

α depends on the anisotropic elastic constants of the crystal (Kaganer *et al.*, 2020). Particularly, for a 110 oriented diamond plate, $\alpha = 0.02$, while for a silicon plate of the same orientation $\alpha = 0.18$. An exceptionally small value for the diamond, which is a result of compensation of the Poisson and the anisotropy effects, gives rise to a little depth dependence of the lattice spacing.

The displacement of atoms due to the bending changes the electron density of the crystal from a periodic function $\varrho(\mathbf{r})$ for a perfect non-bent crystal to $\varrho(\mathbf{r} - \mathbf{u}(\mathbf{r}))$. The Fourier component of the electron density for the actual reflection \mathbf{Q} changes from $\varrho_{\mathbf{Q}}$ to $\varrho_{\mathbf{Q}} \exp[-i\mathbf{Q} \cdot \mathbf{u}(\mathbf{r})]$.

The kinematical diffraction amplitude (3) can be written as an integral over the scattering plane of the crystal

$$f_1 = \int_{-\infty}^{\infty} dx \int_{-D/2}^{D/2} dz \exp(iq_x x + iq_z z - i\mathbf{Q} \cdot \mathbf{u}), \quad (10)$$

where D is the thickness of the crystal plate. We omit here and in the next equation the constant prefactors that are not relevant to our study.

Since the x -dependence of the displacement field of a bent crystal is $x^2/2R$, an x -range relevant to diffraction is comparable with D and the integration over x can be extended to the infinite limits. This integration results in a phase factor which drops out when calculating $|f_1|^2$. In the remaining integral over z , we proceed to a dimensionless variable $\xi = 2z/D$. Then, the integral (10) gives

$$R(\omega' - \omega) = \left| \int_{-1}^1 \exp(i f \xi - i b \xi^2) d\xi \right|^2, \quad (11)$$

where it is denoted

$$b = \frac{\pi \alpha D^2}{4 R d}, \quad f = \pi \frac{D}{d} \frac{\omega' - \omega}{\bar{\omega}}. \quad (12)$$

In deriving dimensionless parameters (12), we take into account that $Q = 2\pi/d$.

The integral (11) can be expressed through cosine and sine Fresnel integrals $C(x)$ and $S(x)$ as

$$R(\omega' - \omega) = \left| F\left(\frac{f+b}{\sqrt{2\pi b}}\right) - F\left(\frac{f-b}{\sqrt{2\pi b}}\right) \right|^2, \quad (13)$$

where $F(x) = C(x) + iS(x)$. Examples of the resolution function calculated by Eq. (13) are presented in Fig. 1. It is however of interest to investigate the dependence of the resolution on the parameters b and f qualitatively.

As long as $b \leq 1$, the quadratic term in the exponent in Eq. (11) can be neglected, and the resolution function is $\text{sinc}^2 f$, where $\text{sinc}(x) = \sin(x)/x$. Then, the resolution by the Rayleigh criterion is simply $\Delta E/E = (\omega' - \omega)/\bar{\omega} = d/D$, cf. Eq. (16) by Kaganer *et al.* (2020). Let us take a 440 reflection from diamond crystal of thickness $D = 20 \mu\text{m}$ bent to a radius of $R = 10 \text{ cm}$ and the X-ray energy of $E = 12 \text{ keV}$ as a reference example. In

this case, shown in Fig. 1(a) by black line, $b = 1$. The resolution $\Delta E = 0.038 \text{ eV}$ is reached due to a small value $\alpha = 0.02$ for diamond.

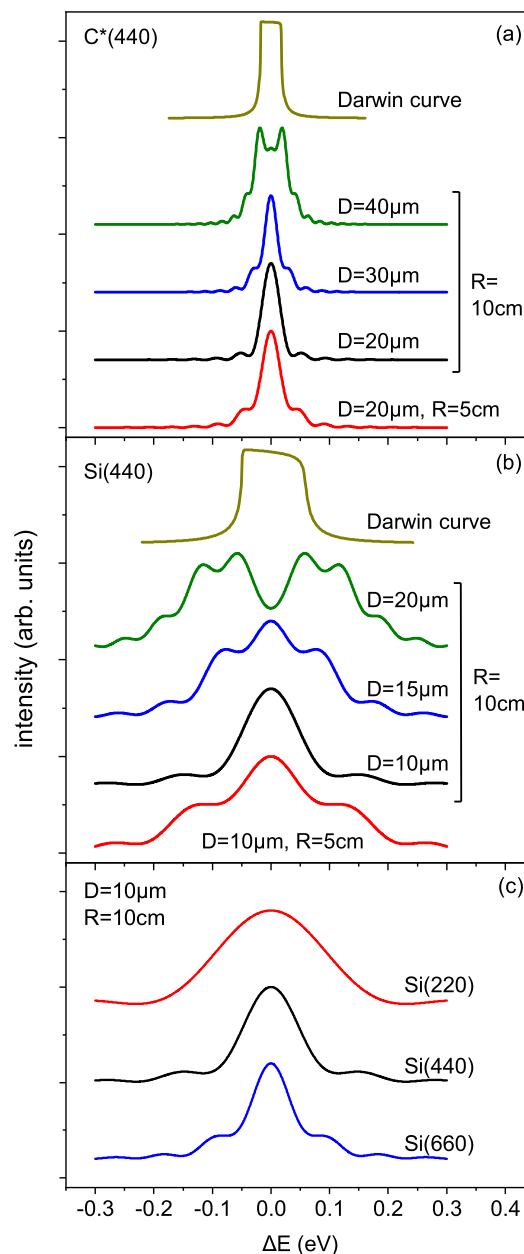


Figure 1

Resolution of a bent-crystal spectrometer at the x-ray energy 12 keV for different bending radii R and crystal thicknesses D for reflection 440 from diamond (a) and silicon (b), and for different reflections from silicon (c). Darwin curves of the respective reflections are shown in (a) and (b).

The top curve in Fig. 1(a) is the Darwin curve of the same reflection, i.e., the rocking curve of dynamical diffraction curve at an infinitely thick non-bent diamond crystal. It corresponds to a resolution that could be obtained in a stationary diffraction experiment by an angular scan of the incoming beam. This resolution is approximately the same as can be reached by kinematical diffraction at a strongly bent crystal (black curve), which

does not require the angular scanning and hence is applicable to detect the spectra of X-ray pulses.

When the bending radius of a 20 μm thick diamond crystal is reduced to 5 cm or the crystal thickness is increased to 30 μm , the value of the parameter b increases to $b = 2$, and the quadratic term in the exponent in Eq. (11) cannot be neglected anymore. The resolution function acquires additional wings, see red and blue lines in Fig. 1(a). If the crystal thickness is increased further to 40 μm , we have $b = 4$. Then, the shape of the resolution function qualitatively transforms, see the olive curve in Fig. 1(a). In this case of $b \gg 1$, the integral (11) can be calculated by the stationary phase method. The two peaks in the resolution function are due to two different depths, above and below the middle plane $z = 0$ of the crystal, where the diffraction takes place depending on the sign of ΔE . A comparison of the curves in Fig. 1(a) shows that one needs to keep $b \leq 1$ to reach an optimum resolution. Both the increase of the curvature and the increase of the crystal thickness can reduce the resolution.

Figure 1(b) shows the calculated resolution functions for Si(440) reflection. The crystal thickness $D = 10 \mu\text{m}$ and the bending radius $R = 10 \text{ cm}$ give $b \approx 1.5$ (black curve). The same range $b \sim 1$ is reached at a smaller thickness compared to the diamond, since $\alpha = 0.18$ for silicon is almost an order of magnitude larger than the respective value $\alpha = 0.02$ for diamond. The resolution is close to the estimate for small b , $\Delta E/E = d/D$, which gives $\Delta E = 0.11 \text{ eV}$.

The top curve is the Darwin curve for Si(440) reflection at the same energy of 12 keV. Similarly to the case of diamond above, the resolution that could be reached by an angular scan in a stationary diffraction experiment occurs approximately the same as can be reached by the kinematical diffraction in a strongly bent crystal. The resolution is three times worse compared to that of the diamond is because of both a smaller thickness of the bent crystal and a larger lattice parameter of silicon.

Both a decrease of the curvature radius to $R = 5 \text{ cm}$ (red curve) or an increase of the crystal thickness to $D = 15 \mu\text{m}$ (blue curve) causes the increase of the parameter b by a factor of 2 and a decrease of the resolution, roughly by a factor of $\sqrt{2}$. When the crystal thickness is increased further to $D = 20 \mu\text{m}$, i.e., the thickness that is optimal for the diamond, the resolution is strongly decreased and the resolution function possesses two peaks (the olive curve). Thus, the difference in the values of the parameter α , i.e., the difference in anisotropic elastic moduli of the crystals, results in a smaller silicon crystal thickness needed to obtain the best available resolution. A smaller thickness, together with a larger lattice parameter of silicon compared with diamond, gives rise to a worse achievable resolution.

Figure 1(c) compares the resolution functions in successive reflection orders of silicon. The parameters providing an optimum resolution for Si(440), $D = 10 \mu\text{m}$ and $R = 10 \text{ cm}$, are used [black curves in Figs. 1(a,b)]. The Si(220) reflection gives $b = 0.73$ and the resolution $\Delta E = 0.23 \text{ eV}$ is worse than that for Si(440) by a factor of 2 because of the two times larger lattice spacing for this reflection. The Si(660) reflection provides

a narrower curve, but the wings arise because of the increased value $b = 2.2$.

4. Spectrometer resolution of the XFEL radiation pulses

Figure 2 compares spectra of the XFEL pulses incident on the bent crystal with the calculated spectra obtained with the bent-crystal spectrometers. We employ the same pulses as used in our former study (Kaganer *et al.*, 2020). The difference is the use of the convolution integral (6) for the time-integrated intensity, instead of a coherent superposition of the wave with different wave vectors. The left plots in Figs. 2(a–d) cover the whole pulse, while the right ones enlarge a 5 eV wide part of the spectrum.

The pulses generated during the SASE process at the European XFEL are simulated with the code FAST (Saldin *et al.*, 1999), which provides a 2D distribution of electric field in real space at the exit of the undulator for each time moment for various parameters of the electron bunch and the undulator. Simulation results are stored in an in-house database (Manetti *et al.*, 2019). The pulses are simulated for the electron energy 14 GeV, photon energy 12.4 keV, and the active undulator length corresponding to the saturation length (Schneidmiller & Yurkov, 2014). Conversion from the time to the frequency domain is performed using the WavePropaGator package (Samoylova *et al.*, 2016), which provides a 2D distribution of electric field for each frequency of the pulse. We use the spectrum at the center of the pulse in the frequency domain, assuming this distribution to be the same across the beam. Two pulses are compared: a 10 fs pulse generated in an undulator of active length 75 m is used in Figs. 2(a,c), while a 42 fs pulse at the undulator length 105 m is used in Figs. 2(b,d).

Each plot in Fig. 2 compares the incident spectrum (thick gray lines) with two diffracted spectra, corresponding to the calculated resolution functions presented in Figs. 1(a,b) by the same colors. Black curves in Figs. 1(a,b) and 2(a–d) correspond to the optimal conditions for the respective reflections: crystal thicknesses $D = 20 \mu\text{m}$ for C*(440) and $D = 10 \mu\text{m}$ for Si(440), and the same bending radius of $R = 10 \text{ cm}$. The olive curves in Figs. 1(a,b) and 2(a–d) correspond to worse resolutions, obtained with the crystal thicknesses $D = 40 \mu\text{m}$ for C*(440) and $D = 20 \mu\text{m}$ for Si(440), keeping the same bending radius of $R = 10 \text{ cm}$.

The 10 fs pulse gives rise to peaks in the spectrum with the characteristic width of 0.35 eV. They are perfectly resolved in the C*(440) reflection in Fig. 2(a) and reasonably well resolved in the Si(440) reflection in Fig. 2(c). Some loss of the resolution can be seen in the case of Si(440). The 42 fs pulse possesses 0.08 eV wide peaks in the spectrum. The spectrum is well resolved in the C*(440) reflection, see Fig. 2(b), even when the crystal thickness is not optimally chosen. The same spectrum is poorly resolved in Si(440) reflection even with the optimal crystal thickness and bending radius, see black line in Fig. 2(d). The worse resolution at a larger crystal thickness (olive line) notably affects the diffracted spectrum.

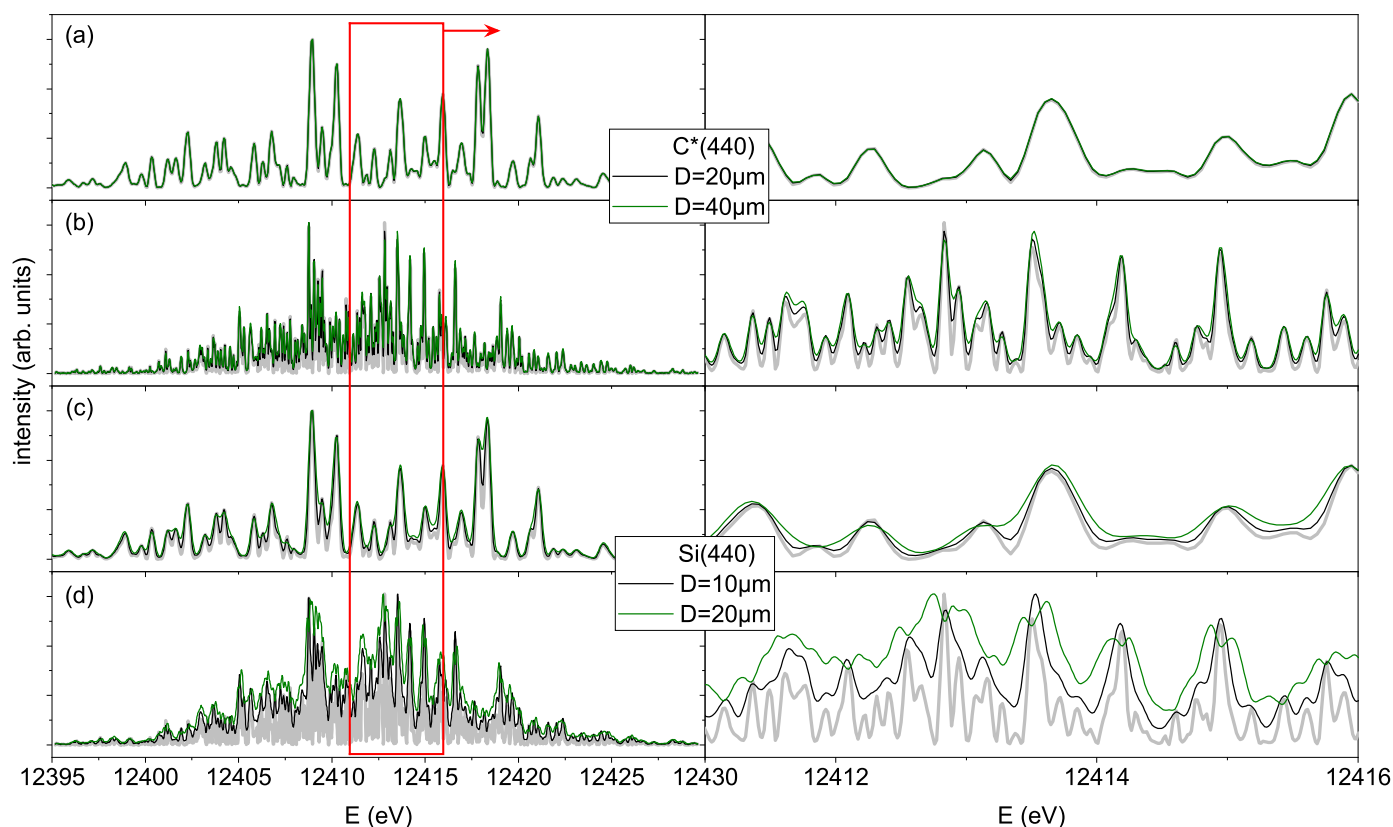


Figure 2

Spectra of 10 fs (a,c) and 42 fs pulses (thick gray lines) and the calculated spectra after diffraction in 440 reflection on (a,b) 20 μm and 40 μm thick diamond and (c,d) 10 μm and 20 μm thick silicon crystal plates. The curvature radius is 10 cm.

5. Conclusions

We have shown that the angular distribution of the intensity diffracted by a bent crystal and integrated over the pulse duration is given by a convolution of the spectrum of the incident X-ray pulse with the resolution function of the bent-crystal spectrometer. The resolution is not affected by the temporal coherence of the pulse.

We have evaluated the resolution of the bent-crystal spectrometer. It is controlled by two parameters. One parameter is the ratio d/D of lattice spacing of the chosen reflection to the thickness of the bent crystal. This ratio is the maximum resolution, $\Delta E/E = d/D$, that is reached if the other parameter, denoted by b , is smaller than 1. The parameter b given by Eq. (12) combines in a single parameter the crystal thickness D , the curvature radius R , the lattice spacing of the actual reflection d , as well as the parameter α representing the anisotropic elastic properties of the crystal.

For $\text{C}^*(440)$ reflection and a crystal thickness of 20 μm , the resolution of $\Delta E/E = 3 \times 10^{-6}$ can be reached. For $\text{Si}(440)$, a smaller thickness required to keep the condition $b \leq 1$, together with a larger lattice spacing of silicon, provide a resolution of $\Delta E/E = 9 \times 10^{-6}$. These results allow to optimize the parameters of the bent-crystal spectrometers for the XFEL radiation pulses.

Acknowledgments

The authors thank Andrei Benediktovitch, Vladimir Bushuev, Leonid Goray, and Ivan Vartanyants for useful discussions and Timur Flissikowski for a critical reading of the manuscript.

References

- Afanasev, A. M. & Kohn, V. G. (1977). *Kristallografiya*, **22**, 622. [Sov. Phys. Crystallogr. **22**, 355 (1977)].
- Boesenberg, U., Samoylova, L., Roth, T., Zhu, D., Terentyev, S., Vannoni, M., Feng, Y., van Driel, T. B., Song, S., Blank, V., Sinn, H., Robert, A. & Madsen, A. (2017). *Optics Express*, **25**, 2852–2861.
- Born, M. & Wolf, E. (2019). *Principles of Optics*. Cambridge: Cambridge University Press.
- Kaganer, V. M., Petrov, I. & Samoylova, L. (2020). *Acta Cryst. A*, **76**, 55–69.
- Landau, L. D. & Lifshitz, E. M. (1984). *Electrodynamics of Continuous Media*. London, U.K.: Pergamon Press.
- Makita, M., Karvinen, P., Zhu, D., Juranic, P. N., Gruenert, J., Cartier, S., Jungmann-Smith, J. H., Lemke, H. T., Mozzanica, A., Nelson, S., Patthey, L., Sikorski, M., Song, S., Feng, Y. & David, C. (2015). *Optica*, **2**, 912–916.
- Manetti, M., Buzmakov, A., Samoylova, L., Schneidmiller, E., Sinn, H., Szuba, J., Wrona, K. & Yurkov, M. (2019). *AIP Conf. Proc.* **2054**, 030019.
- Saldin, E. L., Schneidmiller, E. A. & Yurkov, M. V. (1999). *Nucl. Instrum. Meth. A*, **429**, 233–237.
- Saldin, E. L., Schneidmiller, E. A. & Yurkov, M. V. (2000). *The Physics of Free Electron Lasers*. Berlin: Springer.

Samoylova, L., Boesenberg, U., Chumakov, A., Kaganer, V., Petrov, I., Roth, T., Ruffer, R., Sinn, H., Terentyev, S. & Madsen, A. (2019). *J. Synchr. Rad.* **26**, 1069–1072.

Samoylova, L., Buzmakov, A., Chubar, O. & Sinn, H. (2016). *J. Appl. Cryst.* **49**, 1347–1355.

Schneidmiller, E. & Yurkov, M. (2014). In *Proc.*

FEL2014 Conference, Basel, Switzerland, mop066.
<http://accelconf.web.cern.ch/AccelConf/FEL2014/papers/mop066.pdf>.

Terentyev, S., Blank, V., Kolodziej, T. & Yu. Shvyd'ko (2016). *Rev. Sci. Instr.* **87**, 125117.

Zhu, D., Cammarata, M., Feldkamp, J. M., Fritz, D. M., Hastings, J. B., Lee, S., Lemke, H. T., Robert, A., Turner, J. L. & Feng, Y. (2012). *Appl. Phys. Lett.* **101**, 034103.

Synopsis

Resolution function of a bent-crystal spectrometer for pulses of an X-ray free electron laser is evaluated. Diffraction on a strongly bent diamond single crystal gives rise to a resolution of $\Delta E/E = 3 \times 10^{-6}$, while the strongly bent silicon provides a three times worse resolution.
